文章编号:10069-9941(2018)08-0686-10

Experimental Study and Numerical Simulation of CL-20-Based Aluminized Explosive in Underwater Explosion

FENG Song, RAO Guo-ning, PENG Jin-hua

(*School of Chemical Engineering, Nanjing University of Science & Technology, Nanjing* 210094, *China*)

Abstract: To study the underwater explosion process of hexanitrohexaazaisowurtzitane (CL-20)-based polymer bonded explosives (PBXs) with and without aluminum powders, two kinds of explosives with aluminum contents of 0 and 15% were prepared. An underwater explosion experimental device was designed, and the images of pressure histories, bubble periods and bubble pulse of shock wave were obtained. The shock wave energy, bubble energy and total underwater explosion energy of two kinds of explosives were calculated The underwater explosion process was well-simulated by the AUTODYN software. Results show that when aluminum content increases from 0 to 15%, the total underwater explosion energy increases from 1.4 times TNT equivalent to 1.7 times TNT equivalent. In the process of bubble pulsation, the light is produced in the bubble of CL-20-based aluminized explosive when the time is from 49.5 ms to 49.8 ms. The peak pressure of aluminized explosives and non-aluminized explosives are 15.16 MPa and 15.51 MPa. The bubble of secondary pressure wave are 2.25 MPa and 2.35 MPa, 50.20 ms and 46.76 ms for the bubble periods. The maximum bubble radius are 67.87 cm and 60.27 cm. The simulation results of aluminized explosives and non-aluminized explosives overpressure are 14.90 MPa and 15.14 MPa. The bubble of secondary pressure wave are 2.16 MPa and 2.27 MPa, bubble period for 49.32 ms and 45.90 ms, 66.32 cm and 58.89 cm for the maximum bubble radius. The shock wave and bubble parameters obtained by calculation are in good agreement with experimental results.

Key words: underwater explosion; hexanitrohexaazaisowurtzitane(CL-20); aluminized explosive; shock wave; bubble; numerical simulation

CLC number: TJ55; O384 **Doument code:** A **DOI:** 10.11943/CJEM2017376

1 Introduction

Since the beginning of the Second World War, the research and literature of underwater explosion have been fully studied [1-2]. As the development of modern underwater weapon equipment, the researchers are paying much attention to the issue of how to research and improve the capacity of explosives, enhance the energy release. High energy density material is one of the research hotspots in underwater weapon field.

2,4,6,8,10,12-Hexanitro-2,4,6,8,10,12-hexaazaisowurtzitane was firstly synthesized by Nielsen, commonly known as CL-20[3]. CL-20 is a relatively new energetic compound with high density, good oxygen balance and high explosive power [4-8]. CL-20 is a polycyclic energetic nitramine, because of its superior ballistic, detonation and explosive performance, which may soon replace the monocyclic nitramines RDX and HMX to be the next generation of high-energy material [9-10]. Aluminized explosives are widely used in underwater weapon, which can raise reaction temperature, increase bub-

Received Date: 2017-12-03; **Revised Date:** 2018-01-23

Published Online: 2018-05-08

Project Supported: National Natural Science Foundation For Young Scholars of China(11101091)

Biography: FENG Song(1989-), male, doctor, major in aluminized explosive in underwater explosion.

e-mail:240850587@qq.com

Corresponding author: RAO Guo-ning(1978-), male, lecturer, major in a study of explosion mechanics.

e-mail:njraoguoning@163.com

引用本文:冯淞,饶国宁,彭金华. CL-20基含铝炸药水下爆炸实验研究与数值模拟[J]. 含能材料,2018,26(8):686-695.

FENG Song, RAO Guo-ning, PENG Jin-hua. Experimental Study and Numerical Simulation of CL-20-Based Aluminized Explosive in Underwater Explosion[J]. Chinese Journal of Energetic Materials(Hanneng Cailiao),2018,26(8):686-695.

ble energy. Aluminum particles can react with detonation products under the high pressure and high temperature condition behind the detonation wave, which are usually called secondary reaction [11-12]. Although aluminized explosives have been applied for a long time, the reaction mechanisms of them is still not entirely clear. Because it is difficult to measure how much aluminum reacts with the detonation products behind C-J state and determine the reaction rate. Different computer codes and computational software have been applied to the reaction mechanism by more and more researchers. For example, BKW[13], RUBY[14], TIGER[15], CHEQ[16], JAGUAR[17] and CHEETAH[18] codes, some of them can make good estimates for zero, partial, and full aluminum reaction with the detonation products. Other computer codes and numerical methods are also used to predict performance parameters of aluminized explosives [19-21]. In addition to the above calculation methods, the commercial software such as LSDYNA and AUTODYNA have been widely applied to calculate performance parameters of aluminized explosives in air or water, which include ignition and growth model [22] and Jones-Wilkins-Lee (JWL) [23-25] equation of state (EOS) with a Miller extension for the simulation of aluminized explosives.

The total expansion work of explosives can be calculated by underwater explosion method, which normally is a value close to the heat of explosion or detonation[26]. By computing the shock energy and bubble energy, energy output structure for the underwater explosion can be obtained [27]. Many numerical simulations of underwater explosion have also been conducted in the past few decades, including shock waves[28-29], bubble pulsation[30], structural responses [31-32]. In underwater explosion, the transient load of the bubble pulsation will have great impact on the ship. The researchers are concentrating on understanding the bubble movement. The images of bubble movement are acquired by a high speed video camera and processed by image processing software[33-35].

As said above, we designed an experimental installation to study CL-20-based explosive and CL-20-based aluminized explosive in underwater explosion. The images of bubble of two formulations of the explosives were acquired by a high speed video camera. The bubble of CL-20-based explosive was compared with that of CL-20-based aluminized explosive and the difference between them was discussed.

The paper also investigated the effect of aluminum powder content on shock wave energy, bubble energy and total energy. Compared with conventional explosive(TNT), we did an analysis of the advantage of the total energy of CL-20-based explosive and CL-20-based aluminized explosive. In addition to the experiments, we simulated the process of bubble movement.

2 Experiment

The experiment was conducted in a 2 m×2 m×2 m water tank. The surface height of water in the tank was 1.6 m. The charge was placed at the center 0.8 m below the water surface. The distance between explosion center and pressure transducer was 0.7 m. The high-speed camera was put 1.4 m away from the explosion source. To avoid the influence of reflected shock wave on the bubble pulsation process, a white low impedance material was attached to the wall of the water tank, because the low impedance materials generally have an excellent shock attenuating capacity. Explosion charge, pressure transducer and high-speed camera were located in the same horizontal line. The scheme of the small explosion water tank was shown in Fig.1. In this underwater explosion experiment, CL-20-based explosive and CL-20-based aluminized explosive were used. The mass of each sample is 5 g. The height of each sample is 15 mm. The composition and densities of the charges are listed in Table 1. Every sample was tested twice in parallel.

JO-9159 (95% HMX and 5% binder, 1.860 g·cm^{-3} in density, 1 cm in diameter, 0.5 cm in height, det-

Table 1 Composition and sizes of test samples

sample	composition	height /mm	density/g·cm^{-3}
1#	CL-20/Estane/G/W	14.68	1.929
2#	95/3.5/0.5/1.0	14.68	1.929
3#	CL-20/Al/Estane/G/W	14.21	1.993
4#	80/15/3.5/0.5/1.0	14.20	1.994

onation velocity D = 8862 m·s^{-1}, heat of detonation Q_v = 5.23 kJ·g^{-1}) booster charges of 0.7 g and electric detonator (detonator No. 26) were used for firing. Figure 2 shows the explosive charges of sample 4#.

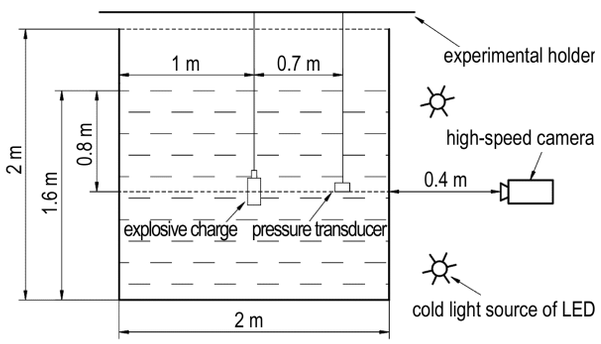

Fig. 1 Schematic diagram of the experimental setup

Fig. 2 Explosive charges of sample 4#

The pressure histories were captured and recorded by an integral circuit piezoelectric crystal pressure transducer (PCB138A05), a sensor signal conditioner (PCB482A20), digital phosphor oscilloscope (Tektronix DPO7104C). The images of bubble pulses were obtained by a high-speed camera (Photron APX-RX) system.

3 Results and Discussion

3.1 Pressure Histories of Shock Wave and Bubble Pulses

Figure 3 present pressure histories of shock wave and bubble pulses measured by sensor placed at the distance of 0.7 m from sample 2# and sample 4#, respectively. The incident shock wave arrived at 327.6 μs, with a peak of value of 15.49 MPa. For CL-20-based aluminized explosive, the incident shock wave arrived at 329.7 μs, with a peak of value of 15.12 MPa. In Fig. 3, it is obvious that the bubble pulsation periods of two samples are 46.76 ms and 50.43 ms.

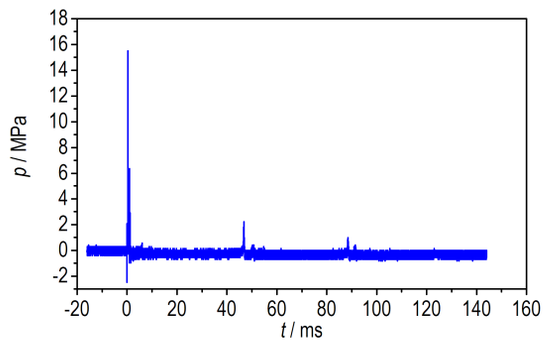

a. sample 2#

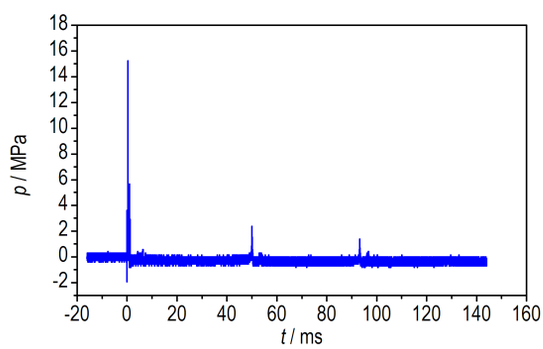

b. sample 4#

Fig. 3 Pressure histories of shock wave measured by sensor placed at the distance of 0.7 m from different samples

3.2 Bubble Motion

Figure 4 shows the bubble generation, expansion and contraction of sample 2#. When the bubble radius reached maximum (t=22.5 ms, R=59.9 cm), the pressure inside the bubble reached minimum. The bubble radius reached minimum at t = 46.5 ms. During the whole moving process of the bubble, the explosion products escaped from the bubble surface.

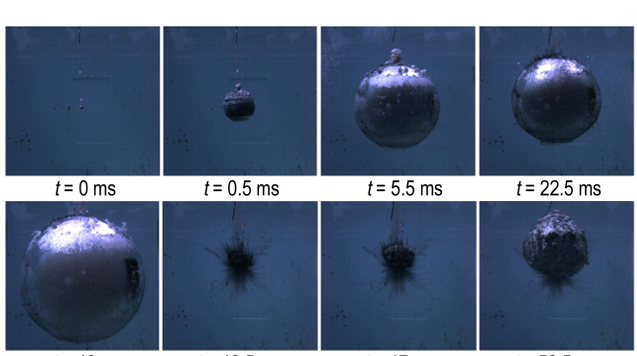

Fig. 4 Experimental pictures of bubble pulse for sample 2#

Figure 5 shows the bubble generation, expansion and contraction of sample 4#. The bubble of maxi-

mum radius was larger with addition of aluminum powder. When the bubble radius reached maximum (t =25.5 ms, R =67.6 cm), the pressure inside the bubble reached minimum. The bubble radius reached minimum at t=50.2 ms. As Fig. 6 shown, when the time was from 49.5 ms to 49.8 ms, the light is produced in the bubble of sample 4#.

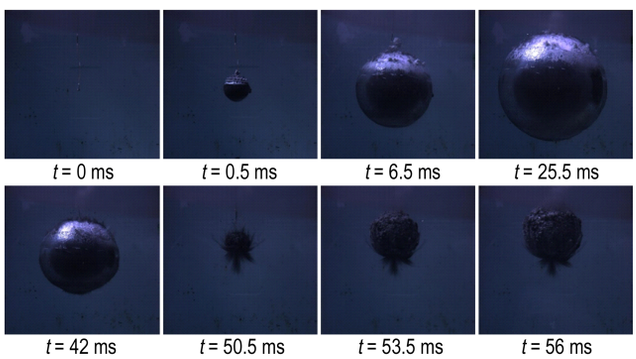

Fig. 5 Experimental pictures of bubble pulse for sample 4#

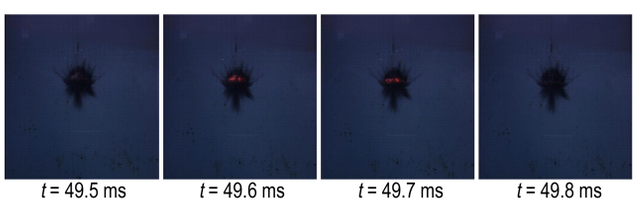

Fig. 6 Experimental pictures of bubble pulse for sample 4#

For aluminized explosive mixtures, the reaction of aluminum particles occurs behind C-J reaction zone[36]. Then, the activated aluminum particles react with detonation products under high temperature and high pressure, which include lots of oxidizing gases, such as H_2O, CO_2, and CO. This is called the secondary reaction of an aluminized explosive [37]. In addition to the above reaction, aluminum particles can react with nitrogen in detonation products to produce aluminum nitride under high temperature and high pressure [38]. The secondary reaction will release energy in the products expansion region after the detonation state for hundreds of microseconds. When the time was from 49.5 ms to 49.8 ms, the secondary reaction was over completely at that time. The light in bubble was caused by high temperature products. Because of aluminum particles can react with explosion products to give out a lot of heat, the temperature of products will rise gradually. When temperature of products reached a certain value, the hotter products generated light. The bubble of CL-20-based explosive had no the secondary reaction. It had no enough heat to make the products generate light.

3.3 Underwater Explosion Energy and Its Calculation

3.3.1 Specific Shock Wave Energy

The shock wave energy released by explosives explosion is related to peak pressure and time of pressure acting. The shock wave formula can be described as follows:

$$p(t) = p_m e^{-t/\theta} \tag{1}$$

Where $p(t)$ denotes the pressure with change of time t, Pa; p_m is the peak pressure in primary shock wave, Pa; θ is the time constant in the shock wave, s. The time constant θ is defined as the time it takes for the pressure to decay from its peak value p_m to value p_m/e, i.e., 0.37 p_m, s.

$$E_s = K_e\left(\frac{4\pi R^2}{\rho_W C_W}\right)\int_0^\tau p(t)^2\,dt \tag{2}$$

$$K_e = 1 + 0.29\gamma + 0.016\gamma^2 \tag{3}$$

$$\gamma = \frac{d}{C_W \cdot \theta} \tag{4}$$

$$e_s = \frac{E_s - E'_s - E''_s}{W} \tag{5}$$

Where K_e is the correction factors of shock wave energy; R denotes the distance from sensor to the center of charge, m; ρ_W is the density of water at charge depth, kg·m^{-3}; C_W is the sound speed of water at charge depth, m·s^{-1}; d is the diameter of pressure-sensitive part of the gage, m; θ is the time constant, s; E_s is the shock energy at measuring point, J; E'_s denotes the shock energy by booster charges at measuring point, J; E''_s is the shock energy by No. 26 electric detonator at measuring point, J; e_s denotes the shock energy per kg explosives at measuring point, J·kg^{-1}; W denotes the charge mass of explosive, kg.

3.3.2 Specific Bubble Energy

The major effects of the bubble generated from

an underwater explosion event take place over a much larger time than of the shock wave. The bubble energy released by explosives explosion is related to the period of the first bubble oscillation. The equation used in calculating the specific bubble energy is expressed as follows:

$$E_b = \frac{1}{8C^3K_1^3}\left[\sqrt{1+4Ct_b\left(\frac{p_h}{p_{hn}}\right)^{\frac{5}{6}}}-1\right]^3 \quad (6)$$

$$e_b = \frac{E_b - E'_b - E''_b}{W} \quad (7)$$

Where C and K_1 are constants at a given charge location in a given pond, t_b is the first bubble period, s; p_h is the total hydrostatic pressure at the charge depth (including atmospheric pressure), Pa; as normalization pressure p_{hn} should use a pressure given by the sum of the normal atmospheric pressure at the surface of the pond (for example 101325 Pa for a sea level site) and the hydrostatic pressure at the chosen charge depth, Pa; E_b is the gas bubble energy at measuring point, J; E'_b denotes the gas bubble energy by booster charges at measuring point, J; E''_b is the gas bubble energy by No. 26 electric detonator at measuring point, J; e_b denotes the gas bubble energy per kg explosives at measuring point, J·kg^{-1}; W denotes the charge weight of explosive, kg.

3.3.3 Specific Total Energy

$$e_t = K_f(\mu e_s + e_b) \quad (8)$$

Where e_t is the total underwater explosion energy per mass unit of an explosive, J·kg^{-1}; K_f is the charge geometry factor, for cylinder shaped charge, K_f =1.08−1.10; μ is the shock loss factor, only relates to the detonation pressure of explosives; More details about these equations can be found in Bjarnholt [26]. In order to get accurate results, a blank test must be conducted only including No. 26 electric detonator and booster charges.

According to the pressure histories of shock wave in Fig.3 and Eqs.(1)−(8) [26], the shock energy, gas energy and total energy of the explosives can be calculated, as shown in Table 2. It is obvious

Table 2 Results of shock energy, gas bubble and total energy

sample	p_m / MPa	θ / μs	T_b / ms	e_s /MJ·kg^{-1}	e_b /MJ·kg^{-1}	e_t /MJ·kg^{-1}
1#	15.52	20.58	46.75	1.13	2.24	5.74
2#	15.49	20.63	46.76	1.13	2.24	5.74
3#	15.20	22.34	49.97	1.31	2.96	7.02
4#	15.12	22.56	50.43	1.31	3.01	7.06

that addition of aluminum powder is of advantage to increase the underwater explosion energy such as shock energy, gas bubble and total energy. The time constant θ of CL-20-based aluminized explosive is larger than that of CL-20-based explosive. The bubble pulse period increases by about 7.4%. The shock wave energy of the CL-20-based aluminized explosive is 1.31 MJ·kg^{-1}, and it is 1.16 times larger than CL-20-based explosive. The bubble energy of the CL-20-based aluminized explosive is 33.3% higher than CL-20-based explosive. These are signs that aluminum powder can greatly improve the bubble energy. The total energy measured at measuring point of CL-20-based aluminized explosive increases by about 27.4%. The total underwater explosion energy per mass unit of an explosive e_t approaches heat of detonation of the explosives[26]. The heat of detonation of the CL-20-based explosive is 5.95 MJ·kg^{-1} [39]. The total underwater explosion energy of CL-20-based explosive is 5.74 MJ·kg^{-1}, and it is 1.4 times larger than TNT (4.09 MJ·kg^{-1}) in underwater explosion energy[40]. Compared with the heat of detonation of the CL-20-based explosive, the error is about 3.5%. The total underwater explosion energy e_t increases by 22.6% with addition of aluminum powder in CL-20. The total underwater explosion energy of CL-20-based aluminized explosive is 1.7 times larger than TNT. But beyond that, the peak pressure in primary shock wave decreases slightly for CL-20-based aluminized explosive. So the addition of aluminum powder can attain the purpose to increase time constant, bubble pulse period and explosion energy. Because aluminum can react with explosion products to give out a lot of heat and gas, decay of pressure slows down and shock energy and total energy increase as

well as gas bubble and pulsation period prolongs.

4 Simulation of the Shock Wave and Bubbles

4.1 Simulation Model

Numerical analysis was based on the explicit finite element program ANSYS AUTODYN. In this article, multi-material Euler solver was used for all of the numerical models including multiple material: the water, air and explosive charges. The model was established based on the actual situation. The dimensions of the water region were set as 2.0 m×1.6 m×2.0 m and those of the air region as 2.0 m×0.4 m×2.0 m using the numerical model. For the portion of the charge and the water near the charge, the mesh size was millimeter magnitude. For the water far from the charge and the portion of the air, the mesh size was centimeter magnitude. The method of transitional mesh division was used in the middle part of the model to reduce the amount of model's nodes and shorten the time of computation. Boundary conditions of the calculation model were "pressure outflow". The simulation of explosion charge was located at a 0.8 m water depth. The booster charges and electric detonator were also taken into consideration. They were converted into explosive energy, which were used in computation program. Hydrostatic pressure gradient depending on water depth was given to all over region of water. The effects of atmospheric pressure, gravitational acceleration during bubble pulsation were also applied to the numerical model.

4.2 Equation of State for Air

Ideal gas equation of state is used for air, and it is given by

$$p = (\gamma - 1)\rho e \tag{9}$$

Where e is the specific internal energy of air, $J \cdot kg^{-1}$; ρ is the density of air, $kg \cdot m^{-3}$; γ is equal to 1.4 in general. Materials parameters of ideal gas EOS for air are shown in Table 3 [41].

Table 3 Material parameters of ideal gas EOS for air

ρ/kg·m^{-3}	γ	e/J·kg^{-1}
1.225	1.4	2.068×10^8

4.3 Equation of State for Water

Polynomial equation of state is used for water, and it is given by

$$\begin{cases} p = A_1\mu + A_2\mu^2 + A_3\mu^3 + (B_0 + B_1\mu)\rho_0 e & \mu > 0 \\ p = T_1\mu + T_2\mu_2 + B_0\rho_0 e & \mu < 0 \end{cases} \tag{10}$$

Where $\mu=\rho/\rho_{ref} - 1$; A_1, A_2, A_3, B_0, B_1, T_1, T_2 are EOS constants. Materials parameters of polynomial EOS for water are shown in Table 4 [41].

Table 4 Material parameters of polynomial EOS for water

A_1/Pa	A_2/Pa	A_3/Pa	B_0	B_1
2.2×10^9	9.54×10^9	1.457×10^9	0.28	0.28
T_1/Pa	T_2/Pa	ρ/kg·m^{-3}	e/J·kg^{-1}	
2.2×10^9	0	1.0×10^3	361.875	

4.4 Equation of State for Explosion Products

To describe the effects of the energy release of the secondary reaction, a time-dependent JWL EOS, in which the late energy released λQ and yielding $\omega(E + \lambda Q)/V$ are added to the energy of the products, is used [25,42], to make it as an improved form to fit for an aluminized explosive. The JWL EOS with Miller extension used for the explosion products is as follows:

$$p = A\left(1 - \frac{\omega}{R_1 V}\right)e^{-R_1 V} + B\left(1 - \frac{\omega}{R_2 V}\right)e^{-R_2 V} + \frac{\omega(E + \lambda Q)}{V} \tag{11}$$

Where p is the pressure, MPa; V is relative volume, m^3; E is relative internal energy of the detonation products, $J \cdot m^{-3}$; A, B, R_1, R_2, and ω are constants, Q and λ are additional specific energy and its reaction rate, $J \cdot m^{-3}$.

$$\frac{d\lambda}{dt} = a(1 - \lambda)^m p^n \tag{12}$$

Where a is the energy release constant, m is the energy release exponent and n is the pressure exponent, λ is the fraction reacted of aluminum powder, these parameters are related to the particle size and specific surface area of aluminum powders [42]. The material parameters are shown in Table 5 [43].

4.5 Numerical Analysis Cases

Because of the limitation of AUTODYN itself, AUTODYN can't show intuitive interface when aluminum reacts with explosion products. The simulation results of the bubble of the CL-20-based alumi-

Table 5 Material parameters of JWL-Miller model for explosives

sample	A/GPa	B/GPa	R_1	R_2	ω	E_0/GJ·m^{-3}
2#	1887.64	162.39	6.5	2.75	0.547	11.50
4#	908.2	12.03	4.77	1.036	0.25	10.20
sample	D/m·s^{-1}	p_{CJ}/GPa	Q/GJ·m^{-3}	a	m	n
2#	9100	40	–	–	–	–
4#	8780	25	4.65	0.028	0.5	0.167

nized explosive had not light inside. So the sample 2# was used as an example. Figure 7 shows the experimental and numerical simulation of bubble pulsation of sample 2#.

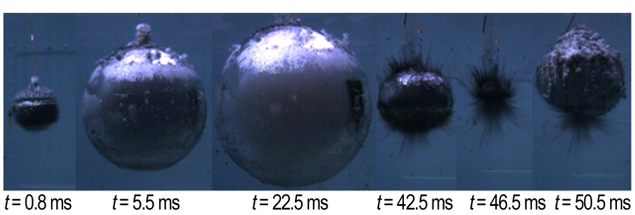

a. experimental

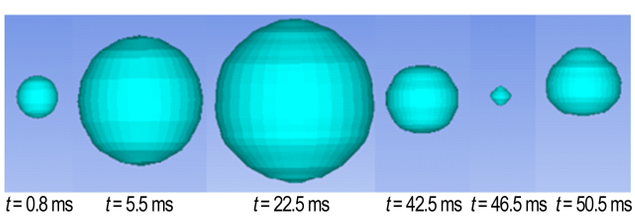

b. simulated

Fig. 7 Comparison of experimental and simulated results for sample 2# about the first pulse of the bubble

During the expansion and collapse, the calculated motion was in excellent agreement with that in experiment. The entire process of bubble pulsation could be clearly and directly observed in the numerical simulation. The simulation results of the bubble pulse properties and bubble pulsation phase were in good agreement with experimental results. Except the light and size, the movement of bubbles between sample 2# and sample 4# were the same. In comparison with experimental values, the explosion products did not escape from the surface of bubble. During the process of bubble pulsation, the experimental results were corresponding with simulation results. Figure 8 and Fig.9 are show that the pressure

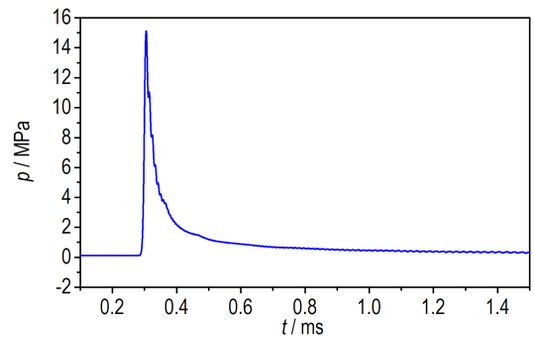

a. shock wave

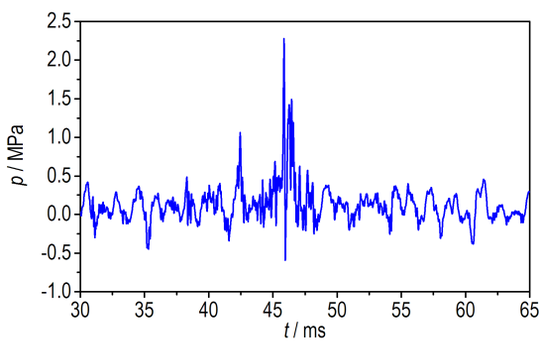

b. bubble pulse

Fig. 8 Pressure histories of shock wave and bubble pulse calculated using AUTODYN at the distance of 0.7 m from the sample 2#

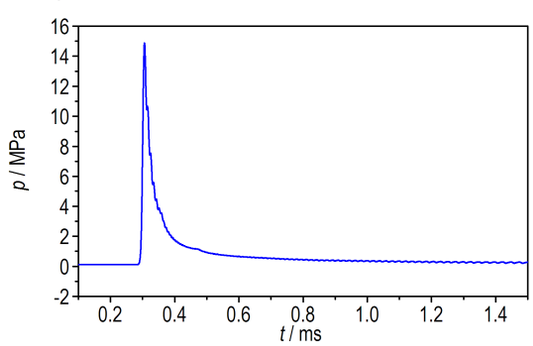

a. shock wave

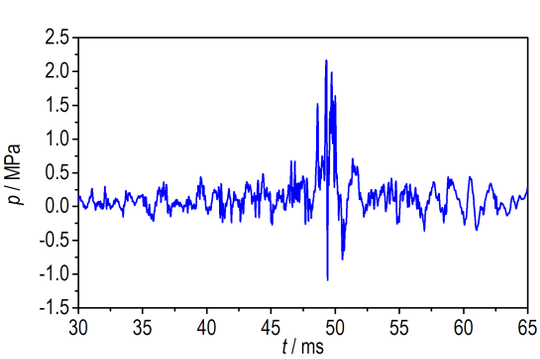

b. bubble pulse

Fig. 9 Pressure histories of shock wave and bubble pulse calculated using AUTODYN at the distance of 0.7 m from the sample 4#

histories of shock wave and bubble pulsation calculated using AUTODYN. From Fig.8a and Fig.9a, we could see that the peak pressure of shock wave in water were 15.01 MPa and 14.80 MPa, respectively. The relative error of the experimental results and numerical ones is 3.10% and 2.12%, respectively.

Table 6 shows the experimental and numerical results for the period, peak pressure and maximum radius of the bubbles and the peak pressure of shock wave. The numerical results of the bubble pulse properties agree with the experimental data, with an average error of bubble period approximately 1.79%, peak pressure of bubble 3.70%, and maximum radius 2.30%. The results of the simulated exam are similar to that of the experimental design which approves the rightness of the numerical model. It implies that the JWL-Miller model could well describe the non-ideal detonation expansion process of the aluminized explosives. In some suitable numerical conditions to the model, it could be reasonably reproduced in shallow underwater explosion about shock wave and bubble pulse.

Table 6 Comparison of the shock wave and bubble pulse properties in the numerical analysis case and in the experiment

sample	peak pressure of shock wave			peak pressure of bubble pulses		
	p_{exp}/MPa	p_{FEA}/MPa	error/%	p_{exp}/MPa	p_{FEA} /MPa	error/%
1#	15.52	15.17	−2.26	2.36	2.27	−3.81
2#	15.49	15.11	−2.45	2.34	2.27	−2.99
3#	15.20	14.92	−1.84	2.27	2.16	−4.84
4#	15.12	14.88	−1.59	2.23	2.16	−3.14
sample	bubble period			maximum radius of bubble		
	t_{exp}/ms	t_{FEA}/ms	error/%	R_{exp}/cm	R_{FEA}/cm	error/%
1#	46.75	45.90	−1.81	60.62	58.89	−2.85
2#	46.76	45.90	−1.84	59.93	58.89	−1.74
3#	49.97	49.32	−1.30	68.11	66.32	−2.63
4#	50.43	49.32	−2.20	67.64	66.32	−1.95

Note: p_{FEA} is peak pressure obtained from finite element analysis.

5 Conclusion

In this paper, we designed an experimental installation to study CL-20-based explosive and CL-20-based aluminized explosive in underwater explosion.

The images of gas bubble in underwater explosion were obtained by high-speed photography. The pictures showed the bubble generation, expansion and contraction. Meanwhile, the difference between CL-20-based explosive and CL-20-based aluminized explosive about bubble had been shown. When the time was from 49.5 ms to 49.8 ms, the bubble of CL-20-based aluminized explosive had light inside, but the CL-20-based explosive had no light in bubble. The point was that the energy released by secondary reactions could heat detonation products.

The pressure histories of shock wave were measured by sensor. After the above methods and results, the different parameters of underwater explosion and underwater explosion energy were obtained. The addition of aluminum powder could attain the purpose to increase time constant, bubble pulse period, maximum radius of bubble and explosion energy. Compared with CL-20-based explosive, the bubble pulse period, maximum radius of bubble, shock wave energy, bubble energy and total underwater explosion energy increase by about 7.4%, 12.6% ,15.9%, 33.3%, 22.6% respectively. The underwater explosive energy of CL-20-based explosive is 1.4 times TNT equivalent. The total underwater explosion energy of CL-20-based aluminized explosive with 15% aluminum is 1.7 times TNT equivalent.

The entire evolution of the bubble was well-sim-

ulated by the AUTODYN software. Computed bubble pulse properties agreed well with measured bubble pulse properties for all cases studied, with an average error of peak pressure of shock wave bubble period approximately 1.79%, peak pressure 3.70%, and maximum radius 2.30%. But the numerical results of bubble images didn't show the light in the bubble. It was different from the experimental images. This simulation work is worth further research.

References:

[1] Cole R H. Underwater explosions[M]. Princeton: Princeton University Press, 1948: 228-233.

[2] Arons A B, Yennie D R. Energy partition in underwater explosion phenomena[J]. *Reviews of Modern Physics*, 1948, 20(3): 519-536.

[3] Nielsen A T. Caged polynitramine compound: U.S. 5693794[P]. 1997.

[4] Geetha M, Nair U R, Sarwade D B, et al. Studies on CL-20: the most powerful high energy material[J]. *Journal of Thermal Analysis and Calorimetry*, 2003, 73(3): 913-922.

[5] Caulder S M, Buess M L, Nock L A. An analytical study of the crystal quality of ε-Hexanitro-hexaazaisowurtzitane (CL-20) synthesized using several different crystallization techniques and intermediate precursors[J]. *Science and Technology of Energetic Materials*, 2005, 66(6): 406-410.

[6] Thangadurai S, Kartha K P S, Sharma D R, et al. Review of some newly synthesized high energetic materials[J]. *Science and Technology of Energetic Materials*, 2004, 65(6): 215-226.

[7] Nielsen A T, Chafin A P, Christian S L, et al. Synthesis of polyazapolycyclic caged polynitramines[J]. *Tetrahedron*, 1998, 54(39): 11793-11812.

[8] Robidoux P Y, Sunahara G I, Savard K, et al. Acute and chronic toxicity of the new explosive CL-20 to the earthworm (Eisenia andrei) exposed to amended natural soils[J]. *Environmental Toxicology & Chemistry*, 2004, 23(4): 1026-1034.

[9] Bolton O, Simke L R, Pagoria P F, et al. High power explosive with good sensitivity: A 2:1 cocrystal of CL-20: HMX[J]. *Crystal Growth & Design*, 2012, 12(9): 4311-4314.

[10] Simpson R L, Urtiew P A, Ornellas D L, et al. CL-20 performance exceeds that of HMX and its sensitivity is moderate[J]. *Propellants, Explosives, Pyrotechnics*, 1997, 22(5): 249-255.

[11] Lewis W K, Rumchik C G, Broughton P B, et al. Time-resolved spectroscopic studies of aluminized explosives: chemical dynamics and apparent temperatures[J]. *Journal of Applied Physics*, 2012, 111(1): 014903.

[12] Manner V W, Pemberton S J, Gunderson J A, et al. The role of aluminum in the detonation and post-detonation expansion of selected cast HMX-based explosives[J]. *Propellants, Explosives, Pyrotechnics*, 2012, 37(2): 198-206.

[13] Mader C L. *Numerical modeling of explosives and propellants*[M]. New York: CRC press, 1998: 33-52.

[14] Levine H B, Sharples R E. Operator's manual for RUBY[R]. UCRL-6815: 1962.

[15] Cowperthwaite M, Zwisler W H. TIGER computer program documentation[R]. ADA002791: 1973.

[16] Nichols A L, Ree F H. CHEQ 2.0 user's manual[R]. UCRL-MA-106754: 1990.

[17] Baker E L, Capellos C, Stiel L I. Jaguar procedures for detonation properties of aluminized explosives[C]//12th International Detonation Symposium, San Diego, California, 2003: 333.

[18] Fried L, Howard W M, Souers P C. Cheetah 2.0 user's manual, lawrence livermore national lab[R]. UCRL-MA-117541: 1998.

[19] Schoch S, Nikiforakis N. Numerical modelling of underwater detonation of non-ideal condensed-phase explosives[J]. *Physics of Fluids*, 2015, 27(1): 281-288.

[20] Donahue L, Zhang F, Ripley R C. Numerical models for afterburning of TNT detonation products in air[J]. *Shock Waves*, 2013, 23(6): 559-573.

[21] Wang X, Hossain K, Jackson T L. The three-dimensional numerical simulation of aluminized composite solid propellant combustion[J]. *Combustion Theory and Modelling*, 2008, 12(1): 45-71.

[22] Wang G, Liu G, Peng Q, et al. A SPH implementation with ignition and growth and afterburning models for aluminized explosives[J]. *International Journal of Computational Methods*, 2017, 14(04): 1750046.

[23] Miller P J, Guirguis R H. Effects of late chemical reactions of the energy partition in non-ideal underwater explosions[C]// AIP Conference Proceedings, Colorado, 1994: 309.

[24] Miller P J. A reactive flow model with coupled reaction kinetics for detonation and combustion in non-ideal explosives[J]. *MRS Online Proceedings Library Archive*, 1995, 418: 413-420

[25] Abe A, Katayama M, Murata K, et al. Numerical study of underwater explosions and following bubble pulses[C]//AIP Conference Proceedings, Cambridge, 2007: 955.

[26] Bjarnholt G. Suggestions on standards for measurement and data evaluation in the underwater explosion test[J]. *Propellants, Explosives, Pyrotechnics*, 1980, 5(2-3): 67-74.

[27] Kowsarinia E, Alizadeh Y, Pour H S S. Experimental evaluation of blast wave parameters in underwater explosion of hexogen charges[J]. *International Journal of Engineering*, 2012, 25(1): 65-72.

[28] Katsabanis P D. Modelling of the underwater shock sensitivity of polyurethane FOAM/PETN explosives[J]. *Journal of Energetic Materials*, 1992, 10(4-5): 189-220.

[29] Lee J, Kuk J H, Cho Y S, et al. Numerical modeling of underwater explosion properties for an aluminized explosive[J]. *Pro-*

pellants, *Explosives*, *Pyrotechnics*, 1997, 22(6): 337-346.

[30] Hsu C Y, Liang C C, Nguyen A T, et al. A numerical study on the underwater explosion bubble pulsation and the collapse process[J]. *Ocean Engineering*, 2014, 81(2014): 29-38.

[31] Klaseboer E, Hung K C, Wang C, et al. Experimental and numerical investigation of the dynamics of an underwater explosion bubble near a resilient/rigid structure[J]. *Journal of Fluid Mechanics*, 2005, 537(2005): 387-413.

[32] Ghoshal R, Mitra N. Underwater explosion induced shock loading of structures: Influence of water depth, salinity and temperature [J]. *Ocean Engineering*, 2016, 126 (2016): 22-28.

[33] ZHAO Sheng-wei, ZHOU Gang, WANG Zhan-jiang, et al. Bubble pulses of small-scale underwater explosion[J]. *Explosion and Shock Waves*, 2009, 29(2): 213-216.

[34] WANG Bin, ZHANG Yuan-ping, WANG Yan-ping. Experimental research of bubble pulsation by underwater explosion method[J]. *Chinese Journal of High Pressure Physics*, 2009, 23(5): 332-337.

[35] HUANG Chao, WANG Bin, YAO Xiong-liang, et al. Laboratory-scale underwater explosion bubble experiment method[J] *Transducer and Microsystem Technologies*, 2011, 30(12): 75-77.

[36] Victorov S B. The effect of Al_2O_3 phase transitions on detonation properties of aluminized explosives[C]//Proc. 12th Int. Detonation Symp, San Diego, 2002: 369-377

[37] SUN Ye-bin, HUI Jun-ming, CAO Xin-mao. Military explosive [M]. Beijing: Weapon Industry Press, 1995: 384-388.

[38] Cook M A, Keyes R T, Horsley G S, et al. A study of the equation of state for ethylenedinitramine[J]. *The Journal of Physical Chemistry*, 1954, 58(12): 1114-1124.

[39] Nan Yu-xiang, JIANG Jian-wei, WANG Shu-you, et al. JWL equation of state of detonation product for CL-20 based pressed composite explosive[J]. *Chinese Journal of Energetic Material* (*Hanneng Cailiao*), 2015, 23(6): 516-521.

[40] Cao W, He Z, Chen W. Measurement of afterburning effect of under oxidized explosives by underwater explosion method [J]. *Journal of Energetic Materials*, 2015, 33(2): 116-124.

[41] ANSYS Inc. AUTODYN user's manual version 11.0 [CP]. 2007.

[42] Miller P J, Guirguis R H.Experimental study and model calculations of metalcombustion in Al/AP underwater explosives [C]//MRS Online Proceedings Library Archive, Boston, 1992: 296.

[43] YANG Kun, CHEN Lang, HU Hong-wei. Effect of content and size of aluminum powder on explosive properties of CL-20 based aluminized explosive [C]//National Symposium on Damage Assessment Technology, Beijing, 2015: 360-368.

CL-20基含铝炸药水下爆炸实验研究与数值模拟

冯 淞,饶国宁,彭金华

(南京理工大学化工学院,江苏 南京 210094)

摘 要: 为了研究含铝粉与不含铝粉的六硝基六氮杂异伍兹烷(CL-20)基高聚物粘结炸药(PBXs)的水下爆炸过程,制备了含铝量分别为0和15%的两种炸药,设计了一个水下爆炸实验装置,得到了炸药的冲击波压力历程、气泡周期和气泡脉动图。计算了两种炸药的冲击波能量、气泡能量和水下爆炸总能量。采用AUTODYN软件模拟了水下爆炸过程。结果表明,当铝含量从0增大到15%时,水下爆炸总能量由1.4倍TNT当量增加到1.7倍TNT当量。气泡脉动过程中,时间从49.5 ms到49.8 ms时,含铝炸药气泡内产生火光。含铝炸药与非含铝炸药超压分别为15.16 MPa与15.51 MPa,气泡二次压力分别为2.25 MPa与2.35 MPa,气泡周期分别为50.20 ms与46.76 ms,气泡最大半径分别为67.87 cm与60.27 cm;仿真得到含铝炸药与非含铝炸药参数超压分别为14.90 MPa与15.14 MPa,气泡二次压力分别为2.16 MPa与2.27 MPa,气泡周期分别为49.32 ms与45.90 ms,气泡最大半径分别为66.32 cm与58.89 cm。实验与仿真结果吻合良好。

关键词: 水下爆炸;六硝基六氮杂异伍兹烷(CL-20);含铝炸药;冲击波;气泡;数值模拟

中图分类号: TJ55; O384 **文献标志码:** A **DOI:** 10.11943/CJEM2017376